Broad boron sheets and boron nanotubes: An *ab initio* study of structural, electronic, and mechanical properties

Jens Kunstmann*
Max-Planck-Institut für Festkörperforschung, Heisenbergstrasse 1, 70569 Stuttgart, Germany

Alexander Quandt
Institut für Physik der Universität Greifswald, Domstrasse 10a, 17489 Greifswald, Germany
(Received 5 January 2006; revised manuscript received 27 March 2006; published 12 July 2006)

Based on a numerical *ab initio* study, we discuss a structure model for a broad boron sheet, which is the analog of a single graphite sheet, and the precursor of boron nanotubes. The sheet has linear chains of *sp* hybridized σ bonds lying only along its armchair direction, a high stiffness, and anisotropic bonds properties. The puckering of the sheet is explained as a mechanism to stabilize the *sp* σ bonds. The anisotropic bond properties of the boron sheet lead to a two-dimensional reference lattice structure, which is rectangular rather than triangular. As a consequence the chiral angles of related boron nanotubes range from 0° to 90°. Given the electronic properties of the boron sheets, we demonstrate that all of the related boron nanotubes are metallic, irrespective of their radius and chiral angle, and we also postulate the existence of helical currents in ideal chiral nanotubes. Furthermore, we show that the strain energy of boron nanotubes will depend on their radii, as well as on their chiral angles. This is a rather unique property among nanotubular systems, and it could be the basis of a different type of structure control within nanotechnology.

DOI: 10.1103/PhysRevB.74.035413 PACS number(s): 61.46.Fg, 73.63.Fg, 81.07.De, 31.15.Ar

I. INTRODUCTION

Boron is an electron deficient element[1] which has a rather fascinating chemistry. Pure boron compounds neither have a purely covalent nor a purely metallic character. This results in a chemical versatility, which is unique among the elements of the periodic table.

The classical bulk modifications of boron are based on B_{12} icosahedra. The simplest boron phase is rhombohedral α-boron,[2] where boron icosahedra are centered on the edges of a rhombohedral unit cell. A different picture arises for boron clusters, where quasiplanar isomers turn out to be more stable than their icosahedral counterparts. This is the consequence of an Aufbau principle for elemental boron clusters postulated by Boustani.[3] This Aufbau principle generally states that stable boron clusters can be constructed from two basic units only: a pentagonal pyramidal B_6 unit and a hexagonal pyramidal B_7 unit,[3] and it implies quasiplanar,[4] tubular,[5,6] convex, and spherical[7] boron clusters. The existence of quasiplanar clusters or "sheets" was recently confirmed by experiment,[8] in perfect agreement with earlier theoretical predictions.[9] Furthermore, the existence of quasiplanar boron clusters implies the formation of boron nanotubes and/or boron fullerenes, because during synthesis, a growing (quasi-)planar boron cluster tends to remove dangling bonds by forming closed tubular or polyhedral modifications. And indeed, recent experimental studies demonstrate the existence of boron nanotubes.[10,11]

Carbon nanotubes[12] on the other hand are a structural paradigm for all nanotubular materials and they can be seen as cylindrical modifications of graphite, which may geometrically be constructed by cutting a rectangular piece out of a single graphene sheet and rolling it up to form a tube. Almost all properties of carbon nanotubes can be derived from the properties of a single graphene sheet, which means that a profound understanding of graphite is the key to understand the basic properties of carbon nanotubes. The same relation holds for boron sheets (BSs) and boron nanotubes (BNTs): understanding the structure and the properties of BSs will be crucial for our understanding of the basic properties of BNTs.

This paper builds on previous work[13,14] to establish such a basic connection between BSs and BNTs, but it should be pointed out that our previous reasoning was mainly based on the individual structures of finite sized quasiplanar boron clusters.[4,15,16] Using *ab initio* structural optimization methods for solid systems we could finally discriminate among different structure models for layered boron compounds and establish a simple model for a broad and stable BS.

After a detailed description of this search process, we will analyze the properties of the most stable structure model. Then we will show how these results may be used to explain the structure, the stability, the electronic, and the mechanical properties of BNTs. In particular the somewhat surprising constriction of zigzag BNTs, which has been reported in a recent publication,[17] may now be clearly understood on the basis of the elastic properties of BSs.

It must be pointed out that up to now, a *broad* BS, which would be the analog of a single graphite sheet, could not be found experimentally. But when writing up this paper we became aware of an interesting work by Evans *et al.*,[18] who consider three BS models and five BNTs of small tube radii, and the work of Cabria *et al.*[19] who study two BS models and three BNTs. Although our results are certainly based on a more extensive search for stable BS and BNTs, our findings for the stable BS are, from a structural and energetic point of view, in excellent agreement with these authors. Thus the present structure model could independently be confirmed by three different groups. However, there is still some disagreement about the ground state structures of BNTs. Lau *et al.*,[20] for example, have recently reported about structures for BS and BNTs, which are very different from

the structure models of Evans *et al.* and Cabria *et al.*, but the present study is in clear favor of the latter.

II. METHODS

As pointed out by Pauling[1] elemental boron has a complicated and rather versatile chemistry. Therefore the only reliable theoretical tools, which may allow for a proper description of boron chemistry, are first principles calculations.[3]

In order to carry out structural optimizations of BSs and BNTs we used the VASP package, version 4.4.6.[21,22] The latter is a density functional theory[23] based *ab initio* code using plane wave basis sets and a supercell approach to model solid materials, surfaces, or clusters.[24] During all of our simulations, the electronic correlations were treated within the local-density approximation (LDA) using the Perdew-Zunger-Ceperley-Alder exchange-correlation functional,[25,26] and the ionic cores of the system were represented by ultrasoft pseudopotentials[27] as supplied by Kresse and Hafner.[28] The k-space integrations were carried out using the method of Methfessel and Paxton[29] in first order, where we employed a smearing width of 0.3 eV.

With the help of the VASP program, one can determine interatomic forces, which may be used to relax the different degrees of freedom for a given decorated unit cell. Eventually one will detect some atomic configurations, which correspond to (local) minima on the total energy landscape. In order to carry out those extensive structure optimizations in a more effective way, we employed a conjugate gradient algorithm,[24] and we allowed all of the atomic coordinates to relax, as well as all but one lattice parameter. This rigid lattice parameter would fix the interlayer separation for BS and the intertubular distance for BNTs at 6.4 Å, which effectively makes them stand-alone objects. The sizes of the k-point meshes for different systems with different unit cells were individually converged, such that changes in the total energy were reduced to less than 3 meV/atom. In the course of a structural optimization run, all interatomic forces were finally reduced to less than 0.04 eV/Å. The cutoff energy for the expansion of the electronic wave functions in terms of plane waves was 257.1 eV for the relaxation runs, and 321.4 eV for a final static calculation of the total energy.

The cohesive energies given in Tables I and II were calculated from

$$E_{\mathrm{coh}} = E_{\mathrm{bind}}/n. \tag{1}$$

E_{bind} is the the atomic binding energy per unit cell and n is the number of atoms per unit cell. Therefore in our definition E_{coh} will be a positive number.

For band structures and the analysis of Fermi surfaces in Sec. III B 2 and Appendix B we used the Stuttgart TB-LMTO-ASA package, which is a density-functional theory[23] based code using short range[30] linearized muffin-tin orbitals[31] within the atomic sphere approximation (ASA). It allows static calculations of the electronic properties for periodic systems. We used the nonspin polarized LDA exchange-correlation functional of Barth and Hedin[32] and a k-mesh of $30\times30\times3$.

TABLE I. Detailed LDA description of the optimized lattice structures of the flat (a) and puckered (b) boron sheets (see Figs. 2 and 3, their bond lengths, cohesive energies E_{coh} [Eq. (1)], and their elastic moduli $C_x=C_{11}$ and $C_y=C_{22}$ obtained after stretching a sheet along the Cartesian x or y direction [Eqs. (2) and (3)].

Sheet	(a) Flat	(b) Puckered
Lattice type	Triangular (2D)	Orthorhombic (3D)
Lattice parameter (Å)	$A=1.69$	$A=2.82$
		$B=1.60$
		$C=$arbitrary
Primitive vectors	$\boldsymbol{a}_1=A\left(\frac{\sqrt{3}}{2},\frac{1}{2}\right)$	$\boldsymbol{a}_1=A(1,0,0)$
	$\boldsymbol{a}_2=A\left(\frac{\sqrt{3}}{2},-\frac{1}{2}\right)$	$\boldsymbol{a}_2=B(0,1,0)$
		$\boldsymbol{a}_3=C(0,0,1)$
Atoms/unit cell	1	2
Atomic position (Å)	$\boldsymbol{R}_1=(0,0)$	$\boldsymbol{R}_1=(0,0,0)$
		$\boldsymbol{R}_2=\left(\frac{1}{2}A,\frac{1}{2}B,0.82\right)$
Bond lengths (Å)	$a_{\mathrm{B\text{-}B}}=1.69$	$a^{\sigma}_{\mathrm{B\text{-}B}}=1.60$
		$a^{\mathrm{diagonal}}_{\mathrm{B\text{-}B}}=1.82$
E_{coh} (eV)	6.76	6.94
Elastic modulus	$C_x=C_y=0.75$	$C_x=0.42$
(TPa)		$C_y=0.87$

III. BORON SHEETS

A. Finding a structure model

Following the Aufbau principle[3] a BS is basically a quasiplanar arrangement of hexagonal pyramidal B_7 units. A planar projection of such a system will always form some kind of triangular lattice (see Fig. 1). However, the out of plane modulation (i.e., the puckering) remains unspecified by the Aufbau principle. The latter has to be determined using *ab initio* structural optimizations, after setting up a suitable supercell that will allow for a systematic generation of various periodic puckering schemes.

The versatile chemistry of boron is reflected in a complicated energy landscape, which is full of local minima. Therefore the standard optimization techniques like the conjugate gradients method used in this study are most likely to find local minima, rather than global minima. Therefore we examined the energy landscape quite carefully by performing *many* optimization runs, which started from quite diverse initial configurations.

The basic puckering schemes were taken from the structures of B_{22}, B_{32}, and B_{46} clusters, which are described in

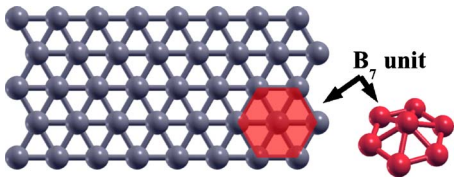

FIG. 1. (Color online) Top view of a quasiplanar boron sheet. In a planar projection the atoms form an almost perfect triangular lattice. The basic structural unit is a hexagonal pyramidal B_7 cluster, as suggested by the Aufbau principle (Ref. 3) (see text).

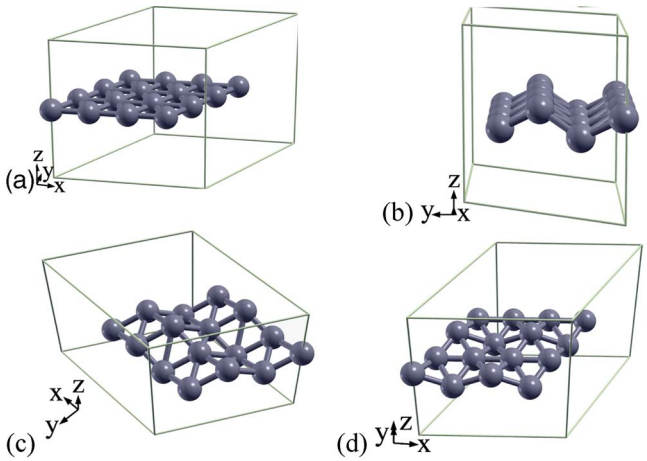

FIG. 2. (Color online) Different structure models for broad boron sheets. Each supercell (thin lines) contains 16 atoms. (a) A simple flat sheet is metastable. (b) A simple up and down puckering seems to be the most stable modulation. Structures (c) and (d) are unstable. Models (b), (c), and (d) are periodic repetitions of structural motives taken from B_{22}, B_{46}, and B_{32} clusters, described in Ref. 4.

Ref. 4. We repeated the puckering periodically in a triangular supercell containing 16 atoms [see Figs. 2(b)–2(d)], and optimized the resulting structures. For the sake of comparison we also examined a flat BS [see Fig. 2(a)].[33] The flat boron sheet (a) occupies a local minimum on the energy landscape with a cohesive energy of 6.76 eV/atom, but small out-of-plane elongations of individual atoms immediately cause a puckering of the BS. This was confirmed by shifting one atom 0.1, 0.2, and 0.4 Å out of plane and reoptimizing the resulting structures. Thus model (a) turns out to be metastable (as also pointed out in Refs. 18 and 19); any thermal vibration would lead to a permanent deformation of a flat boron sheet. Models (c) and (d) are completely unstable, and they both relax to structure (b). In order to scan the energy landscape for other candidate structures we took sheet (a) and shifted each of the 16 atoms out of the plane, employing a random elongation Δz between +0.4 and −0.4 Å. Those structures were reoptimized as before. It turns out that 8 out of 11 optimizations led to model (b), while the remaining three runs resulted in a metastable kinked structure with a cohesive energy of 6.86 eV/atom (see Appendix C).

The fact that models (c) and (d) as well as 8 out of 11 randomly puckered sheets would relax to model (b) means that structure (b) defines a rather pronounced minimum on the energy landscape. The high structural stability of model (b) is confirmed by its high cohesive energy of 6.94 eV/atom, which is the highest cohesive energy of all BSs that we found. We thus conclude that the most suitable structure model for a broad BS will be (b), being 0.18 eV/atom more stable (0.21 and 0.26 eV/atom in Refs. 19 and 18, respectively) than an unrealistic flat BS. The puckering itself seems to be an important mechanism to stabilize the BS,[19] which will be examined in more detail in Sec. III B.

In order to determine the lattice structures of (a) and (b) we performed LDA calculations, where we would fix the unit cell of each system for a series of Cartesian lattice constants A or B, whereas all of the internal (atomic) degrees of freedom were allowed to relax. The resulting total energies for a given set of lattice constants were fitted to polynomial curves $E(A)$ and $E(B)$, from which we determined the equilibrium properties of the systems. The results are summarized in Table I. The diagonal elements of the elastic tensor $C_x=C_{11}$ and $C_y=C_{22}$ may be interpreted as a first approximation to a macroscopic Young's modulus. They were calculated as follows:

$$C_x = \frac{A_0}{Bh}\left(\frac{\partial^2 E(A)}{\partial A^2}\right)_{A_0}, \tag{2}$$

$$C_y = \frac{B_0}{Ah}\left(\frac{\partial^2 E(B)}{\partial B^2}\right)_{B_0}, \tag{3}$$

h is the height of the BS, and it was defined as $h=\Delta z+2R_{\mathrm{vdW}}$; Δz is the puckering height of the sheet and R_{vdW} is the van der Waals radius.[34] A_0 and B_0 are the equilibrium lattice constants.

The optimized planar model (a) seems to form a triangular lattice with one atom per unit cell and a single lattice constant A, which is in the range of a typical boron-boron bond length $A=a_{\mathrm{B\text{-}B}}=1.69$ Å. But within the accuracy of the given methods, we cannot really decide whether the lattice structure is perfectly triangular or slightly less symmetric. Assuming perfect triangular symmetry the two elastic moduli C_x and C_y are equal, and they are surprisingly big: $C_y=C_y \approx 750$ GPa. Which means that even if the flat BS is metastable compared to other model boron sheets, it nevertheless has an extraordinary high stiffness. In Appendix B we will analyze model (a) in more detail.

In Fig. 3 we depicted the unit cell of model (b). It consists of two basis atoms, and its planar projection is almost triangular, but not quite so. It is common to describe such a system with a face centered rectangular unit cell with lattice constants A and B. For $A/B=\sqrt{3}=1.732$ a planar projection of the system would be equivalent to a triangular system. In our case $A/B=1.76$, which is a small, but noticeable departure from triangular symmetry. Due to a puckering height of $\Delta z=0.82$ Å, such a system might best be described using a three-dimensional orthorhombic unit cell. The corresponding lattice parameters and bond lengths can be found in Table I.[55]

B. Properties of the model boron sheet

In this section we will analyze the properties of model (b), which turns out to be the most stable structure for broad BS. Therefore, whenever we write "boron sheet" (BS) in the following, we will only refer to model (b).

In order to compare the BS with a known boron structure we also calculated the cohesive energy of the α boron, which turns out to be 7.51 eV/atom. This corresponds to an energetic difference of 0.57 eV/atom (0.58 and 0.57 eV/atom in Refs. 18 and 19, respectively), which is huge, but one has to take into account that we are comparing a single boron sheet with a bulk reference structure.

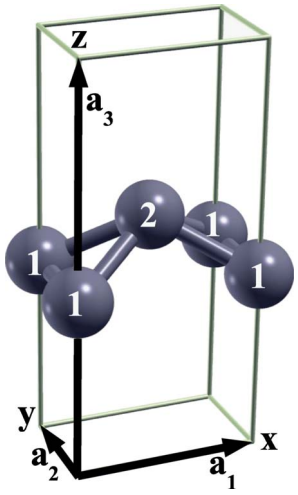

FIG. 3. (Color online) The orthorhombic unit cell of model (b) with two basis atoms (see Table I). In a *xy*-projection atom 1 is located at the corners of a rectangular unit cell, while atom 2 is located at the center of the unit cell. Along the *z* direction the boron atoms will generate a simple up and down puckering, with puckering heights around $\Delta z = 0.82$ Å.

1. Mechanical properties

The elastic modulus of model (b) strongly depends on the stretching directions. In Table. I we roughly find that $C_y \approx 2C_x$. How can one explain those rather obvious anisotropies?

To this end, let us have a look at the charge density of the BS (see Fig. 4). We clearly observe some parallel linear chains of σ bonds lying along the armchair direction. Their bond length is $a^{\sigma}_{\text{B-B}} = 1.60$ Å. At lower densities ($\rho < 0.7\ e/\text{Å}^3$, not displayed) a largely homogeneous distribution with a rather complex shape appears, which may be assigned to multicenter bonding typical for boron materials. An analysis of the electron localization function[36] (ELF) leads to similar results, such that we obtain the following preliminary picture of the bonding: on a first level the sheet is held together by homogeneous multicenter bonds, but on a second level there are strong σ bonds lying only along the armchair direction.

Due to the strong σ bonds, any stretching of the BS along the armchair (=*y*) direction will be much harder than a similar stretching along its zigzag (=*x*) direction, where only the slightly weaker multicenter bonds are involved. These results are quite different from the results of Evans *et al.*, who conjecture that the σ bonds are strong but soft.[18] But here we clearly observe that the σ bonds are strong and stiff. However, other basic findings of Evans *et al.* are in good agreement with our results for flat and puckered BSs.

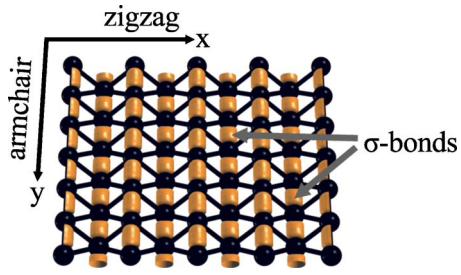

FIG. 4. (Color online) Orange (gray): charge density contours of the boron sheet [model (b)] at 0.9 $e/\text{Å}^3$. One observes parallel linear chains of *sp* hybridized σ bonds lying along the armchair direction.

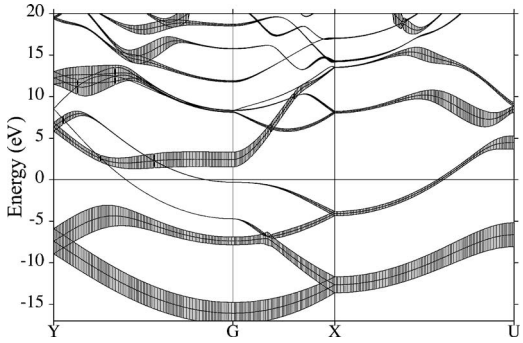

FIG. 5. The band structure of the model BS. The fatness of the bands indicates their *sp* character, and it shows that the σ bonds in Fig. 4 must be of *sp* type. The Fermi energy E_F lies at $E=0$, *G* is the Γ point.

In general the elastic moduli involved are quite high; the stiffness of the σ bonds along the armchair direction is comparable to the stiffness of a graphene sheet. Furthermore, the broken triangular symmetry of the BS's 2D lattice structure, as mentioned in Sec. III A, is another immediate consequence of the anisotropic bond properties.

Evans *et al.* also found that BNTs of different chiralities have different stiffnesses.[18] This can be confirmed by our bonding picture, although our results suggest that zigzag BNTs should be somewhat stiffer than armchair BNTs, while Evans *et al.* noted the opposite (the armchair and zigzag direction are swapped in their and our treatment, see Appendix A 1). We thus conclude that the relation between the microscopic elastic modulus and the macroscopic Young's modulus must be rather complicated in the case of BS and BNTs.

2. Electronic properties

The two-dimensional band structure of the BS $E^{\text{BS}}(k_x, k_y)$ is plotted in Fig. 5 along lines of high symmetry. The BS is metallic, as there are two bands crossing the Fermi energy, which is in perfect agreement with earlier studies of BSs.[13,15]

In order to find out about the hybridization of the σ bonds, we plotted the corresponding amount of *s* and p_y character indicated by the fatness of the bands.[37] We do not find individual dispersions of *s* or *p* bands, and the lowest lying bands show dispersions which *share* *s* and p_y character. That means they are bands consisting of *sp* hybridized orbitals:

$$|sp_a\rangle = \frac{1}{\sqrt{2}}(|s\rangle + |p_y\rangle),$$

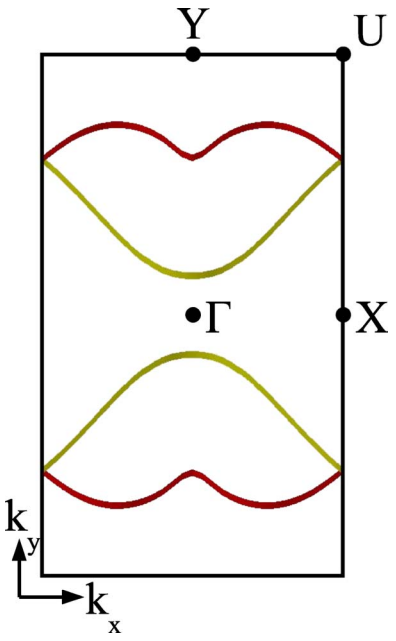

FIG. 6. (Color online) The two-dimensional Fermi surface of the boron sheet. It consists of two contours in red (black) and yellow (gray), which correspond to the two bands crossing the Fermi energy in Fig. 5.

$$|sp_b\rangle = \frac{1}{\sqrt{2}}(|s\rangle - |p_y\rangle).$$

The directional coincidence of the p_y orbitals with the σ bonds in Fig. 4 identifies them to be of sp type. The strength of the σ bonds originates from the fact that the bands lie 5 to 15 eV below the Fermi energy.

The physical picture to describe the multicenter bonds seems to be much more complicated and it is still under investigation (see Appendix B). So far we tried to analyze the multicenter bonds using a simple tight binding model, which comprises the remaining p_x and p_z orbitals as basis states. But it turned out that this treatment can only partially reproduce the conduction bands in Fig. 5; probably a larger basis set is needed.

In Sec. III A we indicated that the puckering has a stabilizing effect for the BS. Now we are in a good position to explain this observation: any flattening of the BS would cause p_x orbitals to interfere with the σ bonds and eventually destroy them. An analysis of the charge density and ELF of a flat BS (see Appendix B) indeed shows that there are no σ bonds involved, but only multicenter bonds.

The existence of sp rather than sp^2 hybridization in a quasi-two-dimensional layered structure is somewhat surprising. Earlier studies of quasiplanar boron clusters[4,16] still presumed the presence of sp^2 hybridization. We think that these assumptions should be reconsidered.

Finally we want to discuss the two-dimensional Fermi surface $E_F = E^{\mathrm{BS}}(k_x, k_y)$ of the BS in Fig. 6. It obviously consists of two contours, which are dispersed throughout the Brillouin zone. This clearly shows the metallic properties of the BS.

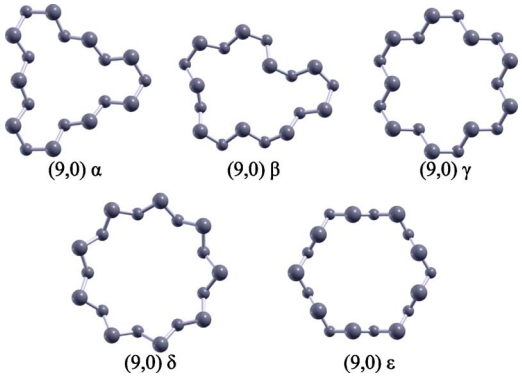

FIG. 7. (Color online) The cross sections of different isomers of a free standing (9,0) zigzag boron nanotube. The big spheres stand for the upper atoms and the small ones for the lower atoms (with respect to the direction of the tube axis). The α and γ isomers are the free standing counterparts of the (9,0)C and (9,0)B tubes in Ref. 17, respectively.

IV. BORON NANOTUBES

In Sec. IV B we will show that the structure of BNTs is strongly related to the structure of the BS, such that the latter may be seen as a direct precursor of BNTs. Therefore it will be interesting to try to characterize BNTs simply by referring to the BS. The mathematical details of such a relation are discussed in Appendix A, and when proceeding along these lines, a BNT may be characterized by two numbers (k,l) with $k,l \geqslant 0$.

For the *ab initio* simulation of BNTs we would start from a series of initial structures with smooth surfaces, which were optimized in a triangular BNT bundle (rope). Here the strong tube-tube interactions (see Sec. IV A) distort the surfaces and naturally induce some puckering. The energy of this configuration is $E_{\mathrm{coh}}^{\mathrm{rope}}$. In order to simulate free standing (individual) BNTs we would then increase the intertubular

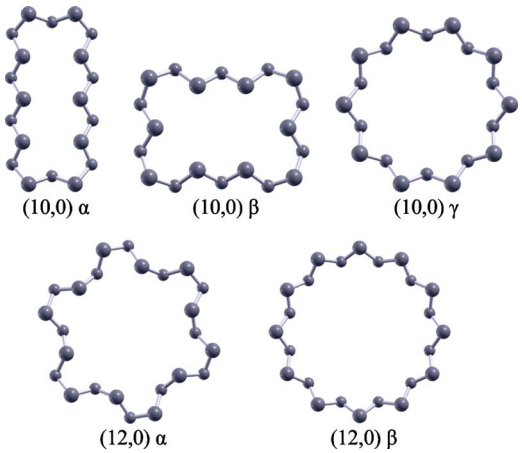

FIG. 8. (Color online) Cross-sectional view of various isomers of free standing (10,0) and (12,0) zigzag boron nanotubes. Again the big spheres mark the upper atoms and the small ones mark the lower atoms. The $(10,0)\alpha$ and $(10,0)\beta$ isomers are free standing counterparts of the (10,0)B and (10,0)C structures in Ref. 17, respectively.

TABLE II. Structural data and energies of different isomers of free standing boron nanotubes: (k,l), (n,m), (i,j): different chiral indices for the same tube type (see Appendix A 1); n: number of atoms per unit cell; Isom.: label of isomer; C_j: rotational symmetry; $a_{\text{B-B}}^{\text{axial}}$, $a_{\text{B-B}}^{\text{diagonal}}$, $a_{\text{B-B}}^{\text{circumferential}}$: boron-boron bond lengths in axial, diagonal, and circumferential direction of a nanotube, the superscript σ indicates that this bond is a σ bond, superscripts σ,i and σ,o refer to inner and outer rings, respectively; $\bar{R}\pm\Delta R$: mean radius of a nanotube [Eq. (4)] and maximal radial variation [Eq. (5)]; $E_{\text{coh}}^{\text{ind}}$: cohesive energy of a free standing (individual) nanotube [Eq. (1)]; $E_{\text{coh}}^{\text{rope}}-E_{\text{coh}}^{\text{ind}}$: this energy is gained when the same nanotube is arranged in a bundle (rope). All energies are given in eV/atom and all lengths are given in Å.

(k,l)	$(n,m)/(i,j)$	n	Isom.	C_j	$a_{\text{B-B}}^{\text{axial}}$	$a_{\text{B-B}}^{\text{diagonal}}$	$a_{\text{B-B}}^{\text{circumferential}}$	$\bar{R}\pm\Delta R$	$E_{\text{coh}}^{\text{ind}}$	$E_{\text{coh}}^{\text{rope}}-E_{\text{coh}}^{\text{ind}}$
(9,0)	(9,0)/(9,9)	18	α	C_3	1.61^{σ}	1.77,1.83,1.86		3.86±1.09	6.93	+0.07
			β	C_1	1.61^{σ}	1.67–1.87			6.92	
			γ	C_3	1.61^{σ}	1.81,1.82		3.83±0.51	6.91	+0.04
			δ	C_9	1.61^{σ}	1.83		4.17±0.39	6.83	
			ϵ	C_3	1.64^{σ}	1.67,1.81		4.39±0.29	6.78	
(10,0)	(10,0)/(10,10)	20	α	C_2	1.60^{σ}	1.79,1.81,1.82,1.87		3.84±1.97	6.91	+0.01
			β	C_2	1.61^{σ}	1.82,1.83,1.84		4.08±1.18	6.90	+0.07
			γ	C_{10}	1.61^{σ}	1.83		4.60±0.41	6.85	
(12,0)	(12,0)/(12,12)	24	α	C_6	1.61^{σ}	1.73,1.83,1.85		5.05±0.65	6.90	+0.02
			β	C_{12}	1.61^{σ}	1.82		5.48±0.41	6.87	+0.05
(0,12)	(4,4)/(12,0)	24	α	C_6		1.69	1.59^{σ},1.69,1.85	2.64±0.68	6.68	+0.3
(0,18)	(6,6)/(18,0)	36	α	C_6		1.70,1.74	1.56^{σ},1.60^{σ},1.71,1.75	4.48±0.57	6.74	+0.27
			β	C_{18}		1.75	1.53^{σ},1.76	4.74±0.34	6.72	
(0,24)	(8,8)/(24,0)	48	α	C_6		1.74,1.75	$1.54^{\sigma,i}$,$1.57^{\sigma,i}$,$1.64^{\sigma,o}$,1.72,1.74	5.99±0.58	6.81	+0.3

distance to 6.4 Å, and optimize those configurations again while keeping the intertubular distances fixed. The energy here is $E_{\text{coh}}^{\text{ind}}$. [$E_{\text{coh}}^{\text{rope}}$ and $E_{\text{coh}}^{\text{ind}}$ are defined after Eq. (1).[38]]

All free standing BNTs are shown in Figs. 7, 8, and 11 and the structural data and energies are collected in Table II. Besides their bond lengths and rotational symmetries we also stated the geometrical mean radius of each tube $\bar{R}$, as well as the maximal radial variation ΔR, which were defined as

$$\bar{R} = \frac{R^{\min} + R^{\max}}{2}, \tag{4}$$

$$\Delta R = R^{\max} - \bar{R} = \bar{R} - R^{\min}, \tag{5}$$

where $R^{\min}$ and $R^{\max}$ are the distances of the innermost and the outermost atoms from the center of the nanotube, respectively.

For many (k,l) BNTs we found more than just one isomer. Therefore each BNT was also given a Greek index which labels different isomers. The latter were ordered according to their cohesive energies, i.e., $(k,l)\alpha$ will denote the most stable isomer, $(k,l)\beta$ would be less stable, and so on.

A. Free standing nanotubes vs nanotube ropes

In Table II the "inter-tubular energy" $E_{\text{coh}}^{\text{rope}}-E_{\text{coh}}^{\text{ind}}$ is the energetic difference between a free standing BNT and its bundled counterpart. One can see that it varies significantly from tube to tube. The intertubular energy seems to depend quite strongly on the structure type, the relative orientations of adjacent tubes in a rope, and the specific type of surface puckering. Furthermore, the intertubular distance in different bundles, which was defined as the minimal separation between two apex atoms on adjacent nanotubes, varies between 1.7 and 3.5 Å in our simulations.

It is obvious that the tube-tube interaction in BNT bundles (ropes) is completely different from what is known from carbon nanotubes, where the intertubular interaction is of van der Waals type. The latter is certainly much weaker, independent of the various structure types, and the intertubular distances are always around 3.4 Å. BNTs on the other hand *may* have *covalent* intertubular bonds,[17,39] and this leads to a decent intertubular bonding energy that depends quite strongly on structural details.

It is interesting to note that the intertubular energy of $(0,l)$ BNTs (armchair types) is significantly higher than for $(k,0)$ BNTs (zigzag). In Sec. IV B 2 we will try to give an explanation for this rather complex bonding scenario.

At this point, it will be worth noting that the original motivation for this paper was a recent study by ourselves, where we reported bundled zigzag BNTs that were somewhat *constricted*[17] (we define the concept of *constriction* at the end of Sec. IV B 1). We conjectured that this constriction would most likely be caused by the arrangement of the tubes in a bundle, where the tube-tube interactions will force the tubes to have geometrical shapes different from free standing BNTs. Now the free standing counterparts of the constricted (9,0)C and (10,0)C BNTs from Ref. 17 are the $(9,0)\alpha$[40] isomer in Fig. 7 and $(10,0)\beta$ in Fig. 8. To our surprise the constriction would *not* disappear after isolating the tube. And even after substantially deforming the $(9,0)\alpha$ structure by homogeneous shrinking, by blowing it up, or by randomly elongating atoms out of their equilibrium position with a maximum amplitude of 0.3 Å, the free standing $(9,0)\alpha$ BNTs would always relax to their constricted forms. This finding is in clear contrast to our previous hypothesis, and it

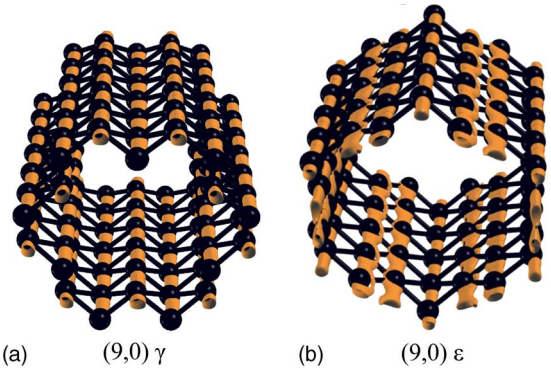

FIG. 9. (Color online) Zigzag boron nanotubes and the presence of straight σ bonds along their axial direction, which are indicated by orange (gray) charge density contours at 0.9 $e/\text{Å}^3$. Due to a lack of stiff σ bonds along the circumferential direction, this type of nanotube might not be stable.

raises the important question where those constrictions finally come from. We will try to give an answer to this question in Sec. IV C.

B. The structure of free standing boron nanotubes

1. Zigzag nanotubes

For zigzag BNTs we found various isomers. Any zigzag BNT may be seen as a BS that was rolled up along its zigzag direction (see Fig. 4 or 14). Thus the linear chains of σ bonds will lie along its axial direction and they will remain straight. These basic bonding properties were typical for *all* zigzag BNT that we studied so far. We just show two typical examples in Fig. 9. Here the bond length of the σ bonds is quite similar to the bond length in the BS, as $a_{\text{B-B}}^{\sigma}=a_{\text{B-B}}^{\text{axial}}=1.61$ Å [the only exception we found was $(9,0)\epsilon$].

The tubes $(9,0)\delta$, $(10,0)\gamma$, and $(12,0)\beta$ are *ideal* BNTs, which denotes the fact that they were initially constructed by a cut and paste procedure described in Appendix A 1, and then reoptimized using *ab initio* methods. Their structure is highly symmetric and we find two bond lengths, which are almost identical to the bond length in the BS. The puckering height $\Delta z=2\Delta R\approx 0.8$ is also quite similar to the BS.

However, an ideal BNT does not seem to be the ground state of a real zigzag BNT, and we found less symmetric isomers that were higher in cohesive energy. It should be noted that zigzag tubes with a smooth surface were not considered here because their cohesive energies are significantly lower than those of puckered BNTs. As an example for the complex shape of zigzag BNTs one may study $(9,0)\epsilon$, which is the least stable isomer of all zigzag BNTs. $(9,0)\epsilon$ has a hexagonal cross section, which probably arises from the triangular supercell into which it was put. Its sides may be seen as parts of a flat BS, whereas the corner pieces are parts of a puckered BS. From Fig. 9 we notice that the σ bonds along the sides are slightly more delocalized than the ones located at the corners. This means that any flattening would destabilize the sigma bonds, and the whole tube is highly metastable. [A similar but squarelike structure was found by Evans *et al.*,[18] which they labeled $(i,j)=(6,6)$, but we think that this structure is highly metastable as well.] Thus the question will no longer be if zigzag BNTs are puckered, but *how* they are puckered.

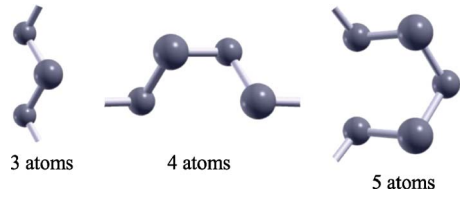

FIG. 10. (Color online) Three basic structure elements. The cross sections of the most stable zigzag boron nanotubes in Figs. 7 and 8 may be composed using these elements, only.

The cross sections of the isomers with a high cohesive energy may be built from three basic structure elements that are shown in Fig. 10. The three-atomic structure element is directly related to the puckering of the BS (compare Fig. 4) whereas the four- and five-atomic elements are just special combinations of three-atomic structure elements. We see that the structure of zigzag BNTs is strongly related to the *local* structure of a simply puckered BS, but their *general* cross-sectional geometries seem to be more complicated and less symmetric than in the simple case of an ideal BNT. This loss of symmetry can also be extracted from the spectrum of diagonal bond lengths, which are associated with multicenter bonds. Those bond lengths are not equal to $a_{\text{B-B}}^{\text{diagonal}}$ of the BS (see Table I), but span a whole range $a_{\text{B-B}}^{\text{diagonal}}\approx 1.7-1.9$ Å.

Some of the most interesting structures are $(9,0)\alpha$, $(9,0)\beta$, and $(10,0)\alpha$, which have cross sections that are far from being circular. Nonetheless they exhibit high cohesive energies Because of the observed unusual shapes of zigzag BNTs we assume that the multicenter bonds obviously possess a high directional flexibility, but at the same time they are also very stiff ($C_x=0.42$ TPa in Table I). Therefore it seems as if these bonds have some jointlike properties, i.e., they are easy to turn, but hard to tear.

In the following we will call a zigzag BNT *constricted*, if it is composed of several five-atomic structure elements. In our work the $(9,0)\alpha$ and the $(10,0)\beta$ isomers are constricted. A constricted zigzag BNT was also found by Evans *et al.*[18] There it is labeled as a $(i,j)=(8,8)$ nanotube, and it corresponds to our $(10,0)\beta$ structure without the two horizontal three-atomic elements.

2. Armchair nanotubes

When rolling up a BS along its armchair direction, the puckered sheet (see Fig. 4) will be transformed into a tube that has inner and outer rings, and the σ bonds will lie along its circumferential direction. On the outer rings the length of the σ bonds will be increased and on the inner rings their length will be reduced. In Fig. 11 we see that for three systems discussed in this study, the σ bonds do really lie along the circumferential direction, and for the (0,18) and (0,24) systems an inner and an outer ring can clearly be identified.

In contrast to zigzag BNTs, for the armchair types we did *not* find several isomers, and we just discuss one ideal BNT, which is the $(0,18)\beta$ isomer. In analogy to zigzag BNTs, we found that this ideal BNT corresponds to a local energy mini-

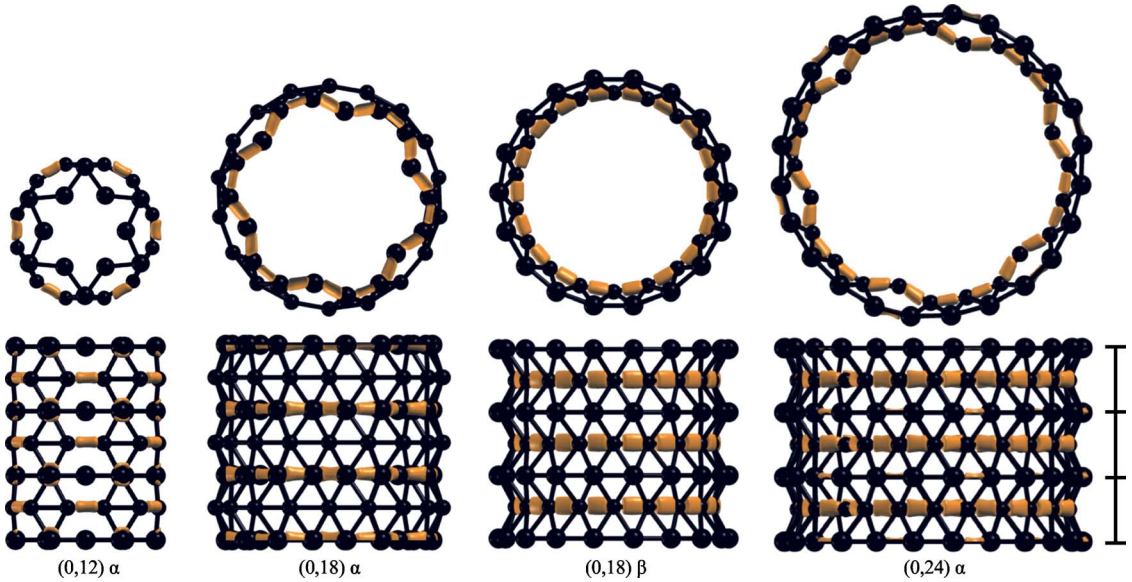

FIG. 11. (Color online) Top and side view of various free standing armchair boron nanotubes and the presence of σ bonds, which are indicated by orange (gray) charge density contours at 0.95 $e/\text{Å}^3$. All armchair nanotubes have bent σ bonds along the circumferential direction, which basically generate the strain energies of the tubes. The black bar on the right indicates the height of a supercell in axial direction that was used for our simulations; for aesthetical reasons we actually displayed three identical units cells.

mum, and the $(0,18)\alpha$ isomer of lower symmetry is 0.02 eV/atom more stable.[41] The latter has σ bonds solely along the inner rings, where the bond lengths are 1.56 and 1.60 Å. Along the outer ring, where the B-B distances (1.71 and 1.75 Å) are significantly longer, the curvature effect has destroyed the σ bonds.[42]

The (0,24) system has similar properties, but here the curvature is smaller, and there are six additional weak σ bonds along the outer rings with a bond length of 1.64 Å. For even larger radii we expect the outer rings of armchair BNTs to develop σ bonds between every single atom.

The radius of the (0,12) BNT is quite small, which makes it extremely difficult for the structure to align its σ bonds. We see that this tube possesses a different geometry, and even along the stiffer rings there are six instead of 12 σ bonds. It is obvious that for armchair BNTs with smaller and smaller radii, the curvature effect will successively destroy the circumferential σ bonds. For the smallest possible BNTs there will probably be no σ bonds at all, and the surface of the tube will become smooth. This agrees with earlier studies by ourselves[5,15] and with the work of Evans *et al.*,[18] where some armchair BNTs of small radii were studied and found to be smooth.

Any destruction of circumferential σ bonds within armchair BNTs of small radii will release electrons that can alter their chemical properties. In Sec. IV A we observed that the intertubular energy for armchair BNT ropes is much higher than for zigzag BNT ropes. Now a possible explanation would be that the released electrons in armchair BNTs induce an enhanced reactivity. In a rope of BNTs, this enhanced reactivity will lead to strong intertubular bonding for armchair BNTs of small radii. In zigzag BNTs the reactivity is lower, as a maximum number of σ bonds can always be achieved, due to the fact that curvature effects will not be able to weaken the axial σ bonds. Therefore we hypothesize that small sized armchair BNTs will have a higher reactivity than zigzag BNTs, and that this reactivity will further decrease with increasing radii.

This reactivity, which leads to the formation of intertubular bonds in BNT ropes, could be very useful when trying to embed BNTs into polymers,[18] where strong chemical bonds between the nanotubes and the polymer matrix are needed in order to improve the mechanical properties of the composite.

C. Strain energy

Let us now compare the cohesive energy of every BNT ($E_{\text{coh}}^{\text{ind}}$ from Table II) with the cohesive energy of the puckered BS ($E_{\text{coh}}^{\text{BS}}$ from Table I). This energy difference will be called strain energy:

$$E_{\text{strain}}(k,l) = E_{\text{coh}}^{\text{BS}} - E_{\text{coh}}^{\text{ind}}(k,l). \tag{6}$$

It is the amount of energy that is needed to roll up a BS into a BNT. The microscopic origin of the strain energy in nanotubes are bent σ bonds along the circumferential direction of the tubes. These bonds have a strong tendency to jump back into a straight orientation, which generates a tension that may be quantified by the strain energy of the systems. Such a tension will stabilize the tubular shape, or to put it more clearly: it will make the nanotube round.

The strain energies of different (k,l) BNTs as a function of their mean radii [Eq. (4)] is plotted in Fig. 12. For the sake of comparison we also show the universal strain energy curve for carbon nanotubes. We call it universal because the strain energy only depends on the radius, but not on the chiral angle (chirality) of the nanotubes: $E_{\text{strain}}^{\text{C}} = E_{\text{strain}}^{\text{C}}(R)$.

As the BNTs are all puckered, there is some variability in the proper choice of a mean tubular radius. Since the strain energy is related to the position of the σ bonds, it makes sense to define the mean radius of armchair BNTs as

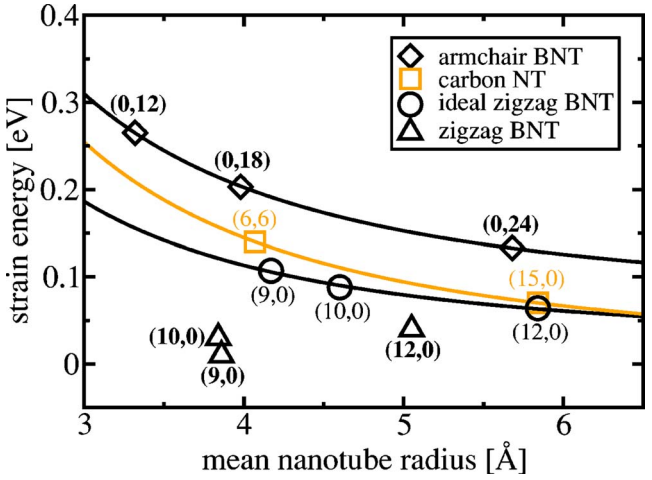

FIG. 12. (Color online) The strain energy of α isomers as a function of the mean radius $\bar{R}$ [Eq. (4)]; for armchair boron nanotubes we used $\bar{R}_\sigma$ [Eq. (7)]. In orange (gray) we show the universal strain energy curve for carbon nanotubes (□); the energy obviously depends on their radii, but not on their chiral angles. For *armchair* boron nanotubes (◇) we find a similar curve, but those boron tubes have more strain energy. For *zigzag* boron nanotubes (△) we cannot really plot a strain energy curve, as different nanotubes of different radii are almost isoenergetic. *Ideal* zigzag boron nanotubes (○) have less strain energy than their armchair counterparts, but they are metastable.

$$\bar{R}_\sigma = \frac{R_\sigma^{\min} + R_\sigma^{\max}}{2}. \tag{7}$$

Here $R_\sigma^{\min}$ and $R_\sigma^{\max}$ are the distances of the innermost and the outermost atoms sharing σ bonds, which is measured from the center of the nanotube.

In earlier works we studied the elasticity of *armchair* BNTs with a tight-binding method[13] and reported a typical strain energy curve lying below the one of carbon nanotubes.[43] Now, using an *ab initio* method, we also found that armchair BNTs have strain energy, but it is higher than for carbon nanotubes.

Different *ideal* zigzag BNTs in Fig. 12 have rather low strain energies. Here none of the σ bonds has to be bent, and the strain energy should only come from the multicenter bonds. But those ideal BNTs are metastable, and isomers of lower symmetry have higher cohesive energies. Thus for the zigzag α isomers no strain energy curve may be plotted as they are more or less isoenergetic. It seems that zigzag BNTs can release some or all of their strain energy by lowering their symmetry and undergo internal deformations (see also Ref. 18), possibly mediated by the jointlike properties of the multicenter bonds.

In summary we see that the strain energy in BNTs is mainly caused by bent σ bonds lying entirely (armchair) or only partially (chiral BNTs) along the circumferential direction. The multicenter bonds are always present, but they seem to have no serious effect on this. The apparent *absence* of strain energy in zigzag BNTs is caused by the fact that the linear σ bonds lie along the axial direction, only. But without smoothing bonding strains, the zigzag tubes are free to take a multitude of cross-sectional morphologies. This explains the number of different isomers that we found for (9,0), (10,0), and (12,0) zigzag BNTs and their bizarre shapes. The constriction of zigzag BNT, first reported in Ref. 17, is a clear consequence of the absence of strained bonds within zigzag BNTs. Armchair BNTs in turn, which are geometrically stabilized by their strain energy, do not seem to have this kind of isomerism.

Chiral BNTs may be thought of as a certain combination of structural elements from armchair and zigzag tubes defined by a certain chiral angle. Therefore we suppose that there will be a separate strain energy curve for every chiral angle lying in-between the armchair and the zigzag curves. The strain energies themselves will depend on the radii and on the chiral angle of a BNT: $E_{\text{strain}}^{\text{B}} = E_{\text{strain}}^{\text{B}}(R, \theta)$. This seems to be a unique property among all nanotubular materials reported so far.

But it remains open whether the strain energy of zigzag BNT will be completely absent, or just significantly smaller than for armchair BNTs. The present results are in favor of the former hypothesis. As carbon nanotubes with large diameters (and very small strain energies) are susceptible to a structural collapse,[44,45] it is possible that without a significant amount of strain energy the zigzag nanotubes could be geometrically *unstable*. Given some thermal fluctuations or strain they might collapse just like big diameter carbon nanotubes. However, such a collapse might also be prevented by a possible energy barrier, which should be proven to be absent in order to support this collapse hypothesis.

Finally we want to point out that the constriction of zigzag BNTs could be an important intermediate mechanism during the possible collapse of a zigzag BNT, which might allow for the formation of B_{12} icosahedra, that are the basic building blocks of all previously known *bulk* boron structures. The five-atomic element (see Fig. 10) forms part of an imaginary zigzag 6-ring, similar to the six apex atoms of a B_{12} icosahedron, as seen along each of its threefold axes.[17]

V. SUMMARY AND CONCLUSIONS

In this paper we studied a number of different structure models for broad boron sheets (BSs). All of them are metallic, and we found that for a 16 atom supercell, the model with a simple up-and-down puckering will be the most stable one. Large quasiplanar boron clusters with a similar structure [B_{22},[4] B_{48},[15] and B_{96}[16]] were already reported before. They may now be understood as a first indication for the onset of periodicity in finite layered boron systems, and thus they are an independent confirmation of the current structure model.

A flat BS has a rather high stiffness, and it seems to be held together primarily by multicenter bonds (see Appendix B). Although the sheet is less stable than previously known bulk phases of boron, as shown here and elsewhere,[18,19] the model sheet could be the ideal theoretical tool for studying complex multicenter bonds.

After describing the lattice structure of the stable BS, we have analyzed its band structure, the corresponding charge densities, and the electron localization function. This would

lead to the following preliminary picture of the chemical bonding: on the one hand the sheet is held together by homogeneous multicenter bonds, on the other hand there are linear *sp* hybridized σ bonds exclusively lying along the armchair direction of the sheet. The existence of *sp* hybridization in quasiplanar BS is somewhat surprising given the fact that earlier studies would always claim sp^2 hybridization. The rather anisotropic bond properties of the sheets lead to different elastic moduli C_x and C_y for stretching the BS in the x and in the y direction. Furthermore, puckering of the BS, which breaks the triangular symmetry, may be understood as a key mechanism to stabilize the *sp* σ bonds. Our results indicate that the sheet analyzed in this study is the boron analog of a single graphene sheet, a possible precursor of boron nanotubes (BNTs), and we wonder whether broad BSs might exist in nature.

Constructing BNTs from the BSs by a cut and paste procedure will generate *ideal* BNTs (see Appendix A). Because the underlying two-dimensional lattice structure is rectangular rather than triangular or hexagonal, it follows that the chiral angle θ ranges from 0° to 90° (θ=0°: zigzag, θ=90°: armchair), and that chiral BNTs do not have an axial translational symmetry. We therefore predict the existence of helical currents in ideal chiral BNTs (Appendix A 2). Furthermore, we presented a band theory for ideal BNTs, employing their helical symmetry, and showed that *all* ideal BNTs are metallic, irrespective of their radius and chiral angle (Appendix A 3). BNTs could therefore be perfect nanowires, superior to carbon nanotubes.

In an independent study of armchair and zigzag BNTs we found that ideal BNTs do not form the ground state of BNTs, and we identified structures of lower symmetry, which are higher in cohesive energy. The symmetries of *real* BNTs still remain to be determined, and the ideal BNTs may be seen as rather close approximants to real BNTs.

We also found that all BNTs, except small radius armchair types, had puckered surfaces, and σ bonds along the armchair direction of the primitive lattice. The existence and mutual orientation of these σ bonds is crucial to understand the *basic* mechanical and energetic properties of BNTs because the strain energy of the tube is mainly generated by bending those σ bonds. The multicenter bonds seem to have no real effect on the strain energy. They are likely to have jointlike properties (they are easy to turn but hard to tear), which allows for a certain flexibility of these bonds, and any bonding strain could immediately be released through internal relaxations.[18]

We showed that armchair BNTs, where the σ bonds lie along the circumferential direction, will have rather high strain energies, whereas zigzag BNTs, where the σ bonds will lie along their axial directions, will have nearly vanishing strain energies. Thus BNTs have a strain energy that depends on the nanotube's radius R as well as on the chiral angle θ: $E^{\mathrm{B}}_{\mathrm{strain}}=E^{\mathrm{B}}_{\mathrm{strain}}(R,\theta)$. We suppose that there will be an individual strain energy curve for every chiral angle lying between the armchair and the zigzag curves. This is a unique property among all nanotubular materials reported so far.

This intriguing feature could even allow for some structure control in nanotechnology. For carbon nanotubes, the strain energies do not depend on their chiralities [$E^{\mathrm{C}}_{\mathrm{strain}}=E^{\mathrm{C}}_{\mathrm{strain}}(R)$], and thus the experimentalists may control the radius, but not the chirality of carbon nanotubes, although the latter will determine the electronic properties of such materials. With the experimental techniques at hand today one might be able to walk along the energy axis by tuning the reaction conditions, and along the radius axis by synthesizing nanotubes within porous templates with well-defined pores sizes. This way it could be possible to synthesize BNTs of a specific type only. The connection to carbon nanotubes may occur via intramolecular junctions,[46] allowing for a controlled layout of carbon nanotubes as well.

The rather low strain energies in *zigzag* BNTs lead to a whole bunch of possible structural isomers, as a nanotube without any significant amount of strain energy will not be able to maintain a circular cross section. This can lead to a certain constriction of zigzag BNTs,[17] and we even hypothesize that zigzag BNTs could be too unstable to really exist out in nature, provided that there will be no significant energy barrier left to prevent a collapse.

Armchair BNTs on the other hand are geometrically stabilized by their strain energies, but for armchair BNTs of rather small radii, the BNTs are unable to maintain a puckered structure necessary to align the circumferential σ bonds. In agreement with earlier studies[5,15,18] we expect them to flatten out and build up a smooth surface. Furthermore, we hypothesize an enhanced reactivity of small radius armchair BNTs in comparison to zigzag BNTs, which could be useful for embedding BNTs into polymers.[18]

ACKNOWLEDGMENTS

For helpful hints and discussions we thank O. K. Andersen (Stuttgart), O. Gunnarsson (Stuttgart), and I. Boustani (Wuppertal). J. Kunstmann gratefully acknowledges support from the International Max Planck Research School for Advanced Materials (IMPRS-AM). We thank A. Kokalj (Ljubljana) for writing the program XCrysDen[47] that was used to generate the atomic structure illustrations.

APPENDIX A: THE MATHEMATICAL DESCRIPTION OF IDEAL BORON NANOTUBES

1. Wrapping vector

The geometrical construction of BNTs from BSs is similar to the construction of carbon nanotubes from a graphene sheet:[35] the basic tubular structure is characterized by a wrapping vector $\boldsymbol{W}$ that defines a rectangular area on the BS, which is rolled up to a cylinder such that $\boldsymbol{W}$ becomes the circumference of the nanotube and its radius will be $R=|\boldsymbol{W}|/2\pi$ (see Fig. 14). We will call any BNT, whose structure may be described by such a construction, an *ideal boron nanotube*.

Due to the fact that a proper structure model for BS was missing for a long time, there remains some confusion in the literature about a proper reference lattice structure. In the work of Cabria *et al.*[19] and in earlier works by us[13,17] (and in full analogy to the construction of carbon nanotubes) the BNTs are related to a honeycomb lattice and defined the wrapping vector $\boldsymbol{W}^{\mathrm{h}}$ as

$$\boldsymbol{W}^{\mathrm{h}} = (n,m) = n\boldsymbol{a}_1^{\mathrm{h}} + m\boldsymbol{a}_2^{\mathrm{h}}, \tag{A1}$$

$\boldsymbol{a}_{1,2}^{\mathrm{h}}$ are the primitive vectors of a honeycomb lattice and n,m are integers. Here each unit cell has one additional atom at the center of the honeycombs, thus consisting of three rather than two atoms (see Fig. 13). Gindulyte *et al.*,[6] Evans *et al.*,[18] and some earlier work of ours[13] relate their BNTs to the simple triangular lattice, having only one atom per unit cell:

$$\boldsymbol{W}^{\mathrm{t}} = (i,j) = i\boldsymbol{a}_1^{\mathrm{t}} + j\boldsymbol{a}_2^{\mathrm{t}}, \tag{A2}$$

$\boldsymbol{a}_{1,2}^{\mathrm{t}}$ are the primitive vectors of a triangular lattice, and i,j are integers. $\boldsymbol{W}^{\mathrm{h}}$ and $\boldsymbol{W}^{\mathrm{t}}$ can be transformed into each other by using[48]

$$(n,m) \mapsto (i,j) = (n+2m, n-m), \tag{A3}$$

$$(i,j) \mapsto (n,m) = \frac{1}{3}(i+2j, i-j). \tag{A4}$$

From Fig. 13 we see that both definitions are based on primitive vectors, which have different orientations.[49] This leads to the rather unsatisfactory situation that armchair and zigzag directions are swapped in both descriptions (see Table II for example). Cabria *et al.* found that all $(n,0)$ zigzag and all $(2n,2n)$ armchair BNTs have puckered surfaces, while the $(2n+1,2n+1)$ armchair tubes shall be smooth due to the fact that an odd number of boron rows along the tube surfaces does not allow for the formation of the simple up and down puckering.[19] We think that these results are not an intrinsic property of BNTs, but rather a consequence of an unsuitable reference lattice system that is unable to properly describe the puckering of the boron sheet, see Fig. 13. Furthermore, the puckering will break the hexagonal symmetry underlying the honeycomb and the triangular lattice.

Therefore we convinced ourselves that these descriptions are not really appropriate to classify BNTs. On the basis of the current BS model we would like to put forward a *different* way of describing BNTs, based on a rectangular lattice underlying the two-dimensional structure of the BS.

We define the wrapping vector $\boldsymbol{W}^{\mathrm{r}}$ as

$$\boldsymbol{W}^{\mathrm{r}} = (k,l) = k\boldsymbol{a}_1^{\mathrm{r}} + l\boldsymbol{a}_2^{\mathrm{r}}, \tag{A5}$$

k,l are integers, and $\boldsymbol{a}_1^{\mathrm{r}} = A(1,0)$ and $\boldsymbol{a}_2^{\mathrm{r}} = B(0,1)$ are the primitive vectors of the rectangular lattice (see Figs. 13 and 3); A and B are the lattice constants from Table I. In analogy to the Dresselhaus construction for carbon nanotubes,[35] we define the chiral angle θ as the angle between the vectors $\boldsymbol{W}^{\mathrm{r}}$ and $\boldsymbol{a}_1^{\mathrm{r}}$, i.e., θ is measured with respect to the zigzag direction coinciding with $\boldsymbol{a}_1^{\mathrm{r}}$ (see Fig. 14).

The categorization of BNTs will be different from other classification schemes because the reduced symmetry of a BS increases the number of possible types of nanotubes, as the range for the chiral angle will be $0° \leqslant \theta \leqslant 90°$, and for the chiral indices (k,l) we find that $k,l \geqslant 0$. Zigzag BNTs will now correspond to $\theta = 0°$ and $(k,l) = (k,0)$, and armchair BNTs will correspond to $\theta = 90°$ and $(k,l) = (0,l)$.

$\boldsymbol{W}^{\mathrm{h}}$ and $\boldsymbol{W}^{\mathrm{t}}$ cannot directly be converted to $\boldsymbol{W}^{\mathrm{r}}$, as they are defined for lattices with different symmetries. For the achiral types, on may use the following analogy (for examples see Table II):

$$\begin{aligned} \text{zigzag: } (k,0)^r &\leftrightarrow (k,0)^h \\ &\leftrightarrow (k,k)^t, \\ \text{armchair: } (0,l)^r &\leftrightarrow (l/3,l/3)^h \\ &\leftrightarrow (l,0)^t. \end{aligned} \tag{A6}$$

2. Translational vector

The *tubular* unit cell of an ideal BNT, being the red (gray) area in Fig. 14, may be defined properly by a wrapping vector $\boldsymbol{W}^{\mathrm{r}}$ [Eq. (A5)] and the so-called translational vector $\boldsymbol{T}$, which is perpendicular to $\boldsymbol{W}^{\mathrm{r}}$:

$$\boldsymbol{T} = (t_1,t_2) = t_1\boldsymbol{a}_1^{\mathrm{r}} + t_2\boldsymbol{a}_2^{\mathrm{r}},$$

$$t_1 = \begin{cases} -\,\mathrm{numerator}(f) & : k \neq 0 \\ 1 & : k = 0, \end{cases}$$

$$t_2 = \begin{cases} \mathrm{denominator}(f) & : k \neq 0 \\ 0 & : k = 0, \end{cases}$$

$$f = \mathrm{reduce}\left(\frac{lB^2}{kA^2}\right). \tag{A7}$$

t_1,t_2 are integers and reduce (r) should indicate that the fraction r must be reduced before determining its numerator and denominator.

Let us consider the length of the translational vector $\boldsymbol{T}$. For the achiral BNTs $|\boldsymbol{T}|$ is particularly small: for all $(k,0)$ zigzag types we have $\boldsymbol{T} = (0,1)$, and for $(0,l)$ armchair BNTs $\boldsymbol{T} = (1,0)$. For the chiral types $\boldsymbol{T}$ depends on the ratio B^2/A^2 [see the last line of Eq. (A7)]. Using $A = 2.819$ and $B = 1.602$ we obtain reduce $(B^2/A^2) = 2\,566\,404/7\,946\,761$. Therefore the coefficients t_1 and t_2 are really huge numbers, which means that $|\boldsymbol{T}|$ becomes macroscopically large. For A and B chosen as above, the estimated length of $\boldsymbol{T}$ for all chiral BNTs will be in the mm range. Imposing some additional symmetry constraints by relating the lattice constants will immediately remedy this problem. For example by choosing $A = \sqrt{3}B$, fraction $(B^2/A^2) = 1/3$, i.e., $|\boldsymbol{T}|$ will be re-

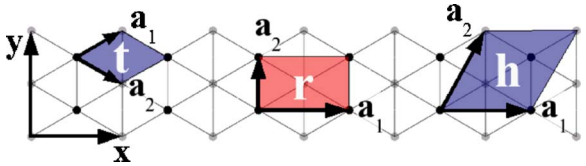

FIG. 13. (Color online) The triangular (t), the rectangular (r), and the honeycomb-derived (h) primitive cells that are used to characterize boron nanotubes. They contain one, two, and three atoms, respectively. Only the rectangular cell may properly describe the puckering of the boron sheet (indicated by black and gray atoms in the background).

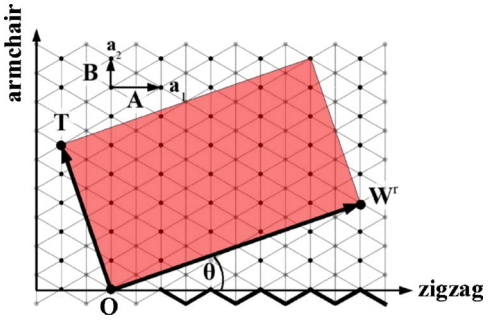

FIG. 14. (Color online) The geometrical construction of an *ideal* boron nanotube from a boron sheet: the red (gray) area is cut and rolled up such that $\boldsymbol{W}^{\mathrm{r}}$ will become the circumference of the nanotube. $\boldsymbol{O}$ is the origin, $\boldsymbol{W}^{\mathrm{r}}$ is the wrapping vector, $\boldsymbol{T}$ is the translational vector, θ is the chiral angle measured with respect to the zigzag direction, $\boldsymbol{a}_{1,2}$ are the primitive vectors of the underlying *rectangular* lattice, and A and B are the lattice constants (see text). The puckering of the boron sheet is indicated by black and gray atoms in the background. The zigzag and the armchair directions are perpendicular to each other. This figure corresponds to $\boldsymbol{W}^{\mathrm{r}}=(5,3)$ and $A/B=\sqrt{3}$, which implies $\boldsymbol{T}=(-1,5)$.

duced to just a few lattice constants (this case was used to generate Figs. 14 and 15). So for the chiral BNTs the specific ratio B^2/A^2 determines the length of the translational vector.

Boron compounds usually have a whole set of different B-B bond lengths, which means that boron does not necessarily favor highly symmetric arrangements. The bond lengths are more flexible than for typical covalent elements like carbon, and the lattice constants A and B of the BS cannot really be seen as fixed parameters; they will have slightly different values in BNTs. Furthermore, the broken planar triangular symmetry of the BS is rather typical for boron, and we should expect that for ideal chiral BNTs, even with different values of A and B, the translational vector might still be large.

To summarize: any departure from triangular symmetry in the BS will create chiral BNTs, which have macroscopically large translational vectors, and achiral types, where $|\boldsymbol{T}|$ is of the order of the lattice constants. Thus achiral BNTs (armchair and zigzag) have a one-dimensional translational symmetry along the tube's axis, which is not present in chiral BNTs. For the latter it might be better to think in terms of helical (chiral) symmetries, only. Therefore we predict the existence of *helical currents* in ideal chiral BNTs. Such currents could lead to very interesting physical effects such as strong magnetic fields[50] and self-inductance effects leading to an inductive reactance[51] of chiral BNTs.

3. Band structure

Within the limit of large nanotube radii, where curvature effects are small, one may derive the one-dimensional band structure of an ideal BNT $E_{\mu}(k')$ by a zone-folding technique,[35] starting from the two-dimensional band structure of a BS $E^{\mathrm{BS}}(k_x,k_y)$. Given the absence of translational symmetry in ideal chiral BNTs, we have to base our zone-folding theory on the helical symmetry of BNTs.[52,53]

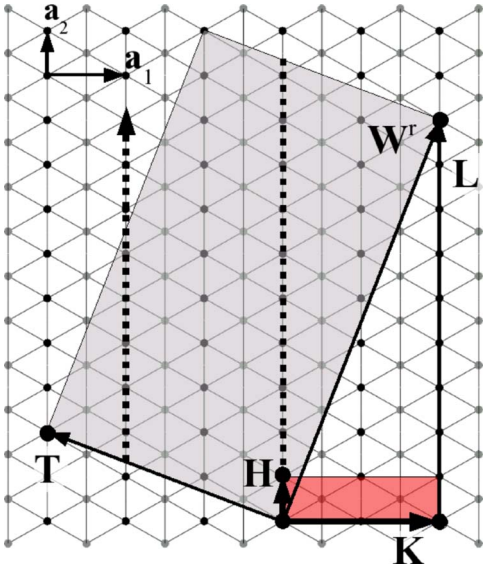

FIG. 15. (Color online) Two different ways of "building up" a nanotube: the *tubular* unit cell in light gray (see also Fig. 14) is repeated along the nanotube's axis, which lies parallel to $\boldsymbol{T}$. The *helical* unit cell in red (dark gray) is translated along spirals (represented by the dotted lines) on the surface of the nanotube; it is defined by the helical vector $\boldsymbol{H}$ and vector $\boldsymbol{K}$. It holds $\boldsymbol{W}^{\mathrm{r}}=\boldsymbol{K}+\boldsymbol{L}$. Here $\boldsymbol{H}=(0,1)$, $\boldsymbol{K}=(2,0)$, and $\boldsymbol{L}=(0,9)$, and therefore $\boldsymbol{W}^{\mathrm{r}}=(2,9)$. The length of $\boldsymbol{T}=(-3,2)$ was artificially reduced by choosing $A/B=\sqrt{3}$.

Figure 15 illustrates that besides constructing a BNT by repeating a *tubular* unit cell one can also build a nanotube by repeating a *helical* unit cell along a spiral winding around the surface of the tube. The direction of this spiral is given by the helical vector $\boldsymbol{H}$[52,53] (in Ref. 35 it is called the symmetry vector $\boldsymbol{R}$), which, when uncoiled into a plane, defines the direction of a translational symmetry [see Eq. (A8) and thereafter]. The helical unit cell is specified by $\boldsymbol{H}$ and the vector $\boldsymbol{K}\perp\boldsymbol{H}$. Furthermore, we define a vector $\boldsymbol{L}\parallel\boldsymbol{H}$, such that $\boldsymbol{W}^{\mathrm{r}}=(k,l)=\boldsymbol{K}+\boldsymbol{L}$ (see Fig. 15).

The helical wave functions are restricted by the following criteria:

$$\Psi_{\mu k'}(\boldsymbol{r}+\boldsymbol{H})=\Psi_{\mu k'}(\boldsymbol{r})\exp(ik'|\boldsymbol{H}|), \tag{A8}$$

$$\Psi_{\mu k'}(\boldsymbol{r}+\boldsymbol{W}^{\mathrm{r}})=\Psi_{\mu k'}(\boldsymbol{r}). \tag{A9}$$

Equation (A8) defines a one-dimensional Bloch state with $-\pi/|\boldsymbol{H}|<k'<\pi/|\boldsymbol{H}|$ and imposes the condition that k' has to be parallel to the reciprocal vector of $\boldsymbol{H}$. Equation (A9) is the tubular boundary condition. In order to construct the helical wave functions $\Psi_{\mu k'}$ we have to use the wave functions of the BS $\Psi_{\boldsymbol{k}}^{\mathrm{BS}}(\boldsymbol{r})$ which have the Bloch property:

$$\Psi_{\boldsymbol{k}}^{\mathrm{BS}}(\boldsymbol{r}+\boldsymbol{R})=\exp(i\boldsymbol{k}\cdot\boldsymbol{R})\Psi_{\boldsymbol{k}}^{\mathrm{BS}}(\boldsymbol{r}), \tag{A10}$$

where $\boldsymbol{R}$ is a vector of the Bravais lattice formed by $\boldsymbol{a}_1^{\mathrm{r}}$ and $\boldsymbol{a}_2^{\mathrm{r}}$. Since the vectors $\boldsymbol{H}$ and $\boldsymbol{W}^{\mathrm{r}}$ are also elements of such a Bravais lattice, Eq. (A8) will automatically be satisfied, and Eq. (A9) together with Eq. (A10) will yield

$$1=\exp[i(\boldsymbol{k}\cdot\boldsymbol{W}^{\mathrm{r}})]. \tag{A11}$$

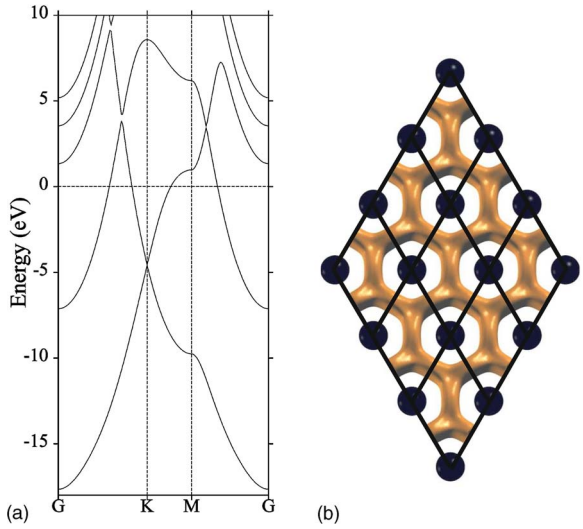

FIG. 16. (Color online) Properties of a flat boron sheet: (a) The two-dimensional band structure. (b) Black lines indicate the triangular unit cells, black spheres are boron atoms, and the orange (gray) contours show the electron localization function (ELF) at contours of 0.7. We observe a simple network of two- and three-center bonds.

In order to proceed, we now have to define the direction of $\boldsymbol{H}$, which may be any Bravais lattice vector.[54] By choosing $\boldsymbol{H}=\boldsymbol{T}$ we recover the case of a tubular unit cell, as described above and in Ref. 35. But in order to make the calculation as simple as possible we assign $\boldsymbol{H}=\boldsymbol{a}_2^{\mathrm{r}}=(0,1)$. Then it follows that $\boldsymbol{K}=(k,0)$ and $\boldsymbol{L}=(0,l)$ (see Fig. 15). As $\boldsymbol{H}\|y$ we have to choose $k'=k_y$. After inserting Eq. (A11) into $E^{\mathrm{BS}}(k_x,k_y)$ we finally obtain the zone-folded band structure of ideal (k,l) $(k\neq 0)$ BNTs as

$$E_{\mu}^{(k,l)}(k') = E^{\mathrm{BS}}\left(\frac{2\pi}{kA}\mu - \frac{lB}{kA}k', k'\right),$$

$$-\frac{\pi}{B} < k' < \frac{\pi}{B},$$

$$\mu = 0, \ldots, k-1. \tag{A12}$$

Equation (A12) will break down for $(0,l)$ armchair BNTs, due to a chiral index $k=0$. But as mentioned before, we are free to choose the direction of $\boldsymbol{H}$, and in such a case we use $\boldsymbol{H}=\boldsymbol{a}_1^{\mathrm{r}}=(1,0)$ and have $k'=k_x$. We thus obtain

$$E_{\mu}^{(0,l)}(k') = E^{\mathrm{BS}}\left(k', \frac{\mu}{l}\frac{2\pi}{B}\right),$$

$$-\frac{\pi}{A} < k' < \frac{\pi}{A},$$

$$\mu = 0, \ldots, l-1. \tag{A13}$$

Unfortunately we do not have an analytical band structure of the BS $E^{\mathrm{BS}}(k_x,k_y)$, yet. But to decide whether a certain ideal BNT is metallic or not we can simply zone-fold the BS's Fermi surface given in Fig. 6. We did so and found that *all* ideal BNTs are indeed metallic, irrespective of their radius and chiral angle. The only ideal BNTs that are not metallic are the (0,1) and the (0,2) types. But these structures are highly unrealistic and we can safely rule them out, as they are not even covered by the Aufbau principle.[3]

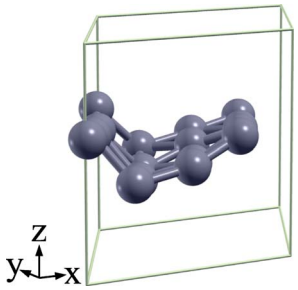

FIG. 17. (Color online) A kinked boron sheet based on a supercell (thin lines) that contains 16 atoms (see text). Apart from the kink its surface is slightly puckered.

APPENDIX B: A FLAT BORON SHEET

The lattice structure, the cohesive energy, and the elastic moduli of the flat boron sheet—model (a)—can be found in Table I. The elastic modulus of $C_{11}\approx 750$ GPa is comparable to graphite. The electronic charge density is nearly uniform in the interstitial region, and the band structure [see Fig. 16(a)] is similar to the band structure of a free electron gas. These results seem to indicate some metallic bonding, as pointed out by Evans *et al.*,[18] but such a picture cannot really account for the planarity and the high elastic modulus of the flat BS. A different qualitative picture of the chemical bonding is obtained after looking at the electron localization function[36] (ELF) in Fig. 16(b). Here we observe a simple network of two- and three-center bonds being less localized (ELF$\approx$0.7) than typical sigma bonds (ELF$\approx$0.9), which are absent here. Thus the flat BS seems to be held together predominantly by multicenter bonds similar to the ones found in pure boron compounds. The chemical understanding of these multicenter bonds is still very limited. We think that, despite of its apparent metastability, model (a) could be an ideal theoretical tool to extend our present understanding of the nature of multicenter bonding in boron.

APPENDIX C: A KINKED BORON SHEET

In Sec. III A we described the optimization of randomly puckered BSs. It is surprising that despite the high complexity of the boron energy landscape for small boron clusters, which are known to have many local minima, these runs seem to have only two possible "attractors." One is model (b)—a simply puckered BS—the other is the kinked BS displayed in Fig. 17. The kinked BS has a metallic density of states and a cohesive energy of 6.86 eV/atom, which is somewhat intermediate between model (a) and model (b). We think that this structure is likely to be an artifact of the finite size of the supercell that we used for the simulation runs, but being an "attractor" of the optimization runs it is still interesting enough to be mentioned here.

*Electronic address: j.kunstmann@fkf.mpg.de

[1] L. Pauling, *Nature of the Chemical Bond* (Cornell University Press, Ithaca, 1960).

[2] M. Fujimori, T. Nakata, T. Nakayama, E. Nishibori, K. Kimura, M. Takata, and M. Sakata, Phys. Rev. Lett. **82**, 4452 (1999).

[3] I. Boustani, Phys. Rev. B **55**, 16426 (1997).

[4] I. Boustani, Surf. Sci. **370**, 355 (1997).

[5] I. Boustani and A. Quandt, Europhys. Lett. **39**, 527 (1997).

[6] A. Gindulyte, W. N. Lipscomb, and L. Massa, Inorg. Chem. **37**, 6544 (1998).

[7] I. Boustani, J. Solid State Chem. **133**, 182 (1997).

[8] H. J. Zhai, B. Kiran, J. Li, and L. S. Wang, Nat. Mater. **2**, 827 (2003).

[9] I. Boustani, A. Rubio, and J. A. Alonso, Chem. Phys. Lett. **311**, 21 (1999).

[10] D. Ciuparu, R. F. Klie, Y. Zhu, and L. Pfefferle, J. Phys. Chem. B **108**, 3967 (2004).

[11] B. Kiran, S. Bulusu, H. J. Zhai, S. Yoo, X. C. Zeng, and L. S. Wang, Proc. Natl. Acad. Sci. U.S.A. **102**, 961 (2005).

[12] S. Iijima, Nature (London) **354**, 56 (1991).

[13] I. Boustani, A. Quandt, E. Hernandez, and A. Rubio, J. Chem. Phys. **110**, 3176 (1999b).

[14] A. Quandt and I. Boustani, ChemPhysChem **6**, 2001 (2005).

[15] I. Boustani and A. Quandt, Comput. Mater. Sci. **11**, 132 (1998).

[16] I. Boustani, A. Quandt, and A. Rubio, J. Solid State Chem. **154**, 269 (2000).

[17] J. Kunstmann and A. Quandt, Chem. Phys. Lett. **402**, 21 (2005).

[18] M. H. Evans, J. D. Joannopoulos, and S. T. Pantelides, Phys. Rev. B **72**, 045434 (2005).

[19] I. Cabria, M. J. López, and J. A. Alonso, Nanotechnology **17**, 778 (2006).

[20] K. C. Lau, R. Pati, R. Pandey, and A. C. Pineda, Chem. Phys. Lett. **418**, 549 (2006).

[21] G. Kresse and J. Furthmüller, Comput. Mater. Sci. **6**, 15 (1996).

[22] G. Kresse and J. Furthmüller, Phys. Rev. B **54**, 11169 (1996).

[23] W. Kohn and L. J. Sham, Phys. Rev. **140**, A1133 (1965).

[24] M. C. Payne, M. P. Teter, D. C. Allan, T. A. Arias, and J. D. Joannopoulos, Rev. Mod. Phys. **64**, 1045 (1992).

[25] J. P. Perdew and A. Zunger, Phys. Rev. B **23**, 5048 (1981).

[26] D. M. Ceperley and B. J. Alder, Phys. Rev. Lett. **45**, 566 (1980).

[27] D. Vanderbilt, Phys. Rev. B **41**, 7892 (1990).

[28] G. Kresse and J. Hafner, J. Phys.: Condens. Matter **6**, 8245 (1994).

[29] M. Methfessel and A. T. Paxton, Phys. Rev. B **40**, 3616 (1989).

[30] O. K. Andersen and O. Jepsen, Phys. Rev. Lett. **53**, 2571 (1984).

[31] O. K. Andersen, Phys. Rev. B **12**, 3060 (1975).

[32] U. von Barth and L. Hedin, J. Phys. C **5**, 1629 (1972).

[33] The initial in-plane boron-boron distance was 1.6 Å. The k-point mesh was $4\times4\times2$ for the optimization runs and $6\times6\times4$ for a final static calculation.

[34] The definition of h looks somewhat arbitrary, as a different definition for h or different van der Waals radii will certainly alter the values for the elastic moduli. But in a test calculation for a single graphite sheet, where we used $\Delta z=0$ (no puckering) and $R^{\mathrm{C}}_{\mathrm{vdW}}=1.7$ Å, we found $C_{11}=C_{22}$ to be 1.08 TPa, in excellent agreement with the literature values of $C_{11}=1.06$ TPa (Ref. 35. For boron we would used $R^{\mathrm{B}}_{\mathrm{vdW}}=1.7$ Å and $\Delta z=0.82$ (see below and Table I). Thus for model (a) we find that $h=3.4$ Å, whereas for model (b) we find that $h=4.22$ Å.

[35] R. Saito, G. Dresselhaus, and M. S. Dresselhaus, *Physical Properties of Carbon Nanotubes* (Imperial College Press, London, 1998).

[36] A. D. Becke and K. E. Edgecombe, J. Chem. Phys. **92**, 5397 (1990).

[37] The orientation of the p_x, p_y, and p_z orbitals coincides with the orientation of the coordinate systems in Figs. 3 and 4.

[38] The k-space integration for free standing BNTs was carried out on a $1\times1\times15$ mesh for zigzag tubes and on a $1\times1\times10$ mesh for armchair types.

[39] A. Quandt, A. Y. Liu, and I. Boustani, Phys. Rev. B **64**, 125422 (2001).

[40] For the $(9,0)\alpha$ BNT the intertubular distance was increased to only 4 Å.

[41] The C_6 symmetry of all α isomers is probably not an intrinsic property, but rather caused by the fact that they were simulated in a triangular supercell.

[42] The diagonal bond lengths $a^{\mathrm{diagonal}}_{\mathrm{B\text{-}B}}$ (which connect the inner and the outer rings) are always shorter compared to the BS (compare Tables I and II); we found them to be in the range $a^{\mathrm{diagonal}}_{\mathrm{B\text{-}B}}\approx1.69-1.75$ Å.

[43] In Ref. 13 smooth BNTs and a flat BS were compared.

[44] N. G. Chopra, L. X. Benedict, V. H. Crespi, M. L. Cohen, S. G. Louie, and A. Zettl, Nature (London) **337**, 135 (1995).

[45] J. A. Elliott, J. K. W. Sandler, A. H. Windle, R. J. Young, and M. S. P. Shaffer, Phys. Rev. Lett. **92**, 095501 (2004).

[46] J. Kunstmann and A. Quandt, J. Chem. Phys. **121**, 10680 (2004).

[47] A. Kokalj, Comput. Mater. Sci. **28**, 155 (2003).

[48] These relations are obtained from: $\boldsymbol{a}^{\mathrm{h}}_1=\boldsymbol{a}^{\mathrm{t}}_1+\boldsymbol{a}^{\mathrm{t}}_2$ and $\boldsymbol{a}^{\mathrm{h}}_2=2\boldsymbol{a}^{\mathrm{t}}_1-\boldsymbol{a}^{\mathrm{t}}_2$.

[49] For the plot in Fig. 13 we used $A=\sqrt{3}B$. This induces triangular symmetry into a rectangular lattice, and the primitive vectors are $\boldsymbol{a}^{\mathrm{h}}_1=\boldsymbol{a}^{\mathrm{r}}_1=\sqrt{3}B(1,0)$, $\boldsymbol{a}^{\mathrm{h}}_2=\sqrt{3}B(\frac{1}{2},\frac{1}{2}\sqrt{3})$, and $\boldsymbol{a}^{\mathrm{t}}_1=B(\frac{\sqrt{3}}{2},\frac{1}{2})$, $\boldsymbol{a}^{\mathrm{t}}_2=B(\frac{\sqrt{3}}{2},-\frac{1}{2})$.

[50] V. M. K. Bagci, O. Gülseren, T. Yildirim, Z. Gedik, and S. Ciraci, Phys. Rev. B **66**, 045409 (2002).

[51] Y. Miyamoto, A. Rubio, S. G. Louie, and M. L. Cohen, Phys. Rev. B **60**, 13885 (1999).

[52] C. T. White, D. H. Robertson, and J. W. Mintmire, Phys. Rev. B **47**, 5485 (1993).

[53] P. J. Lin-Chung and A. K. Rajagopal, J. Phys.: Condens. Matter **6**, 3679 (1994).

[54] In the most general case the zone-folded band structure of ideal BNTs is given by $E_\mu(k')=E^{\mathrm{BS}}(k'\boldsymbol{G_H}/|\boldsymbol{G_H}|+\mu\boldsymbol{G_K})$, with $\boldsymbol{G_H}$ and $\boldsymbol{G_K}$ being the reciprocal lattice vectors of $\boldsymbol{H}$ and $\boldsymbol{K}$, respectively, $-\pi/|\boldsymbol{H}|<k'<\pi/|\boldsymbol{H}|$, $\mu=0,\ldots,N-1$, and $N=|\boldsymbol{H}\times\boldsymbol{K}|/|\boldsymbol{a}^{\mathrm{r}}_1\times\boldsymbol{a}^{\mathrm{r}}_2|$ (Ref. 35).

[55] $a^{\mathrm{diagonal}}_{\mathrm{B\text{-}B}}=a^{\mathrm{1\text{-}2}}_{\mathrm{B\text{-}B}}$ is the bond length between atom 1 and 2, and $a^{\sigma}_{\mathrm{B\text{-}B}}=a^{\mathrm{1\text{-}1}}_{\mathrm{B\text{-}B}}=a^{\mathrm{2\text{-}2}}_{\mathrm{B\text{-}B}}=B$ is the bond length between two equivalent atoms in different unit cells.